ZIBELINE INTERNATIONAL PUBLISHING

Earth Sciences Malaysia (ESMY)

DOI : http://doi.org/10.26480/esmy.02.2019.23.31

ISSN: 2521-5035 (Print)
ISSN: 2521-5043 (online)
CODEN : ESMACU

RESEARCH ARTICLE

AMBIENT SEISMIC NOISE FOOTPRINTS AND SPECTRA IN THE MIDDLE BENUE TROUGH, NIGERIA

Clifford N. C. Mbachi[1], Etim D. Uko[1*], Chibuogwu L. Eze[2], Iyeneomie Tamunobereton-ari[1], Dorathy B. Umoetok[1] and Allu A. Umbugdau[3]

[1]Department of Physics, Rivers State University, PMB 1080, Port Harcourt, Nigeria.
[2]Institute of Geosciences and Space Technology, Rivers State University, PMB 1080, Port Harcourt, Nigeria.
[3]Department of Geology, Nasarawa State University, PMB 1022, Keffi, Nigeria.
**Corresponding Author Emails: cliffmbachi@gmail.com; e_uko@yahoo.com; tamunoberetonari@yahoo.com; chibuogwueze@yahoo.com; dorababbs@gmail.com; umbugaduallu@nsuk.edu.ng*

ARTICLE DETAILS

Article History:

Received 02 August 2019
Accepted 29 September 2019
Available Online 25 October 2019

ABSTRACT

Ambient noise was analysed from a two-dimensional (2D) seismic data acquired in the Middle Benue Trough, Nigeria for the purpose of characterizing the ambient seismic noise. Sercel 428XL recording instrument was deployed on 3 traverse lines where dynamite explosive sources and geophone detectors were used. The acquired data was processed using frequency wavenumber (FK) and wild amplitude attenuation (WAA) algorithms. The dominant amplitude of the primary reflection ranges between -20dB and -10dB, while those of the ambient seismic noise varies between -42dB and -3dB. The primary reflections have dominant frequency varying from 6Hz to 75Hz while that of ambient seismic noise varies between 4Hz and 70Hz. Analysis of the noise shows two distinct ground roll modes with velocities between 400 ms^{-1} and 810 ms^{-1} both of which are dispersive with wavelength (λ) of 61.5m and peak frequency at 6.5Hz. Analysis of passive noise records acquired showed that ambient seismic (background) noise level excluding source-generated noise average of 91.56% are below 25μV, which is the tolerance noise level limit. The combination of frequency wavenumber FK and WAA filters effectively attenuated the surface waves especially ground rolls and other high amplitude noise making the primary reflection very visible and better enhanced. The filtered amplitude values estimated from signal-to-noise (SNR) analysis using cross correlation (XC) method are much higher than the values of the unfiltered amplitudes indicating that SNR are highest when noises are attenuated from the data than when noise algorithm is not applied to the data. The attributes of these seismic noises will provide further information and solution for their suppression during seismic data acquisition and processing.

KEYWORDS

Seismic, signal, noise, frequency, amplitude, Middle Benue Trough, Nigeria.

1. INTRODUCTION

Seismic exploration is a geophysical method that uses a controlled seismic source to generate impulsive sound waves that propagate in the earth's interior. When any source is used to generate seismic energy, the result is many kinds of waves - body, surface wave, air wave, and ambient noise; all at the same time. Seismic noise falls into two broad categories: coherent noise which is the energy that can be predictable from trace to trace across a group of traces while random noise is not predictable from trace to trace. Example of coherent noise are Rayleigh and Love ground rolls, direct wave and refraction. Incoherent (random) noise or ambient seismic noise comprises vibrations caused by sources such as turbulent wind, sea tides, water waves striking the coast, industrial machinery, human and animal activities, trains and cars [1-5].

Afegbua and Ezomo include instrument noise, plant-leaves rustling, debris from shot falling to the ground, movement of the streamer through the water, distant storms, rain drops, atmospheric phenomena, ocean waves as well as installed seismic equipment [6-10]. The air blast noise resulting from source energy is also ambient noise. Other sources of ambient noise are aircraft, earthquake, built-up areas, power line, vehicular traffic including trekking and animal movement, water pumps, quarries and factory [7,8]. Ambient noise obscures the signals and degrade the overall signal quality obtained. As depicted in Figure 1, this random noise is present at the beginning of any acquired data (the pre-shot noise). Coherent and ambient random noises can be observed on seismograms (Figure 2).

Many scholars have reported fascinating results of ambient seismic noise studies in the study area and in the Niger Delta, Nigeria. Most of these studies majored only on the ground roll and weathered-layers characteristics [11-19]. This present work will provide information on the characteristics of ambient seismic noises, their spectra, and their attenuation. The knowledge of the characteristics of ambient seismic noise is essential to future receiver-array design and acquisition parameters of high-quality signals in the study area.

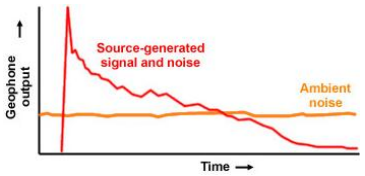

Figure 1: Schematic profile of source-generated signal, noise, and ambient noise [20].

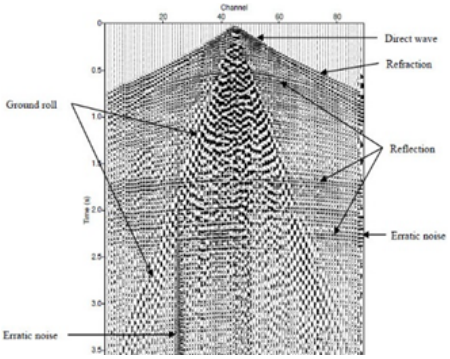

Figure 2: A raw seismic record from a land 2-D seismic project [21].

2. AREA OF THE STUDY AND ITS GEOLOGY

The study area, located in Nasarawa State in the Middle Benue Trough (Figure 3), covers Latitudes 07.50° - 08.50° N and Longitudes 08.00 and 09.30°E. The Benue Trough is an intra-cratonic rift basin which has boundary with Chad Basin in the north and Niger Delta in the south [18, 22-25].

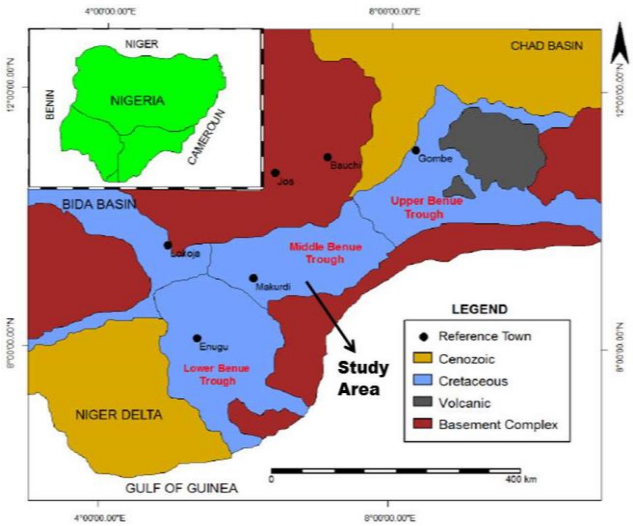

Figure 3: Map of Benue Trough of Nigeria [26].

3. MATERIALS AND METHODS

3.1 Data and Equipment Used

The data used was acquired while carrying out a routine two-dimensional (2D) seismic survey (Figure 4). The energy source utilized was dynamite while the detector was geophone. The spread was made up of 800 groups of geophones and two strings of nine geophones in series. Charge size per hole is 0.4kg in a 4m-hole interval is 3m; source pattern length is 18m; source point interval is 30m (Figure 5) depth of 4m. Shot holes were each loaded with 0.4kilograms of explosives, totalling 2.8 kilograms per source point. Each source hole is thoroughly tamped with earth to reduce hole-blowout and prevent source-generated noise. The seismic data was acquired with a Sercel 428XL instrument.

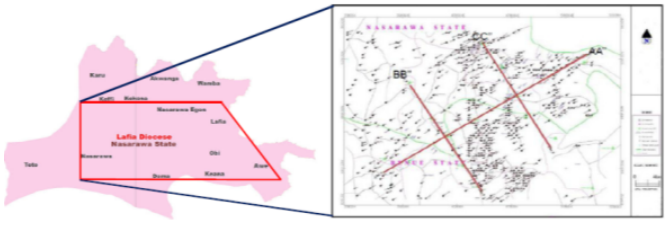

Figure 4: Map of the Study Area showing the Traverse Lines

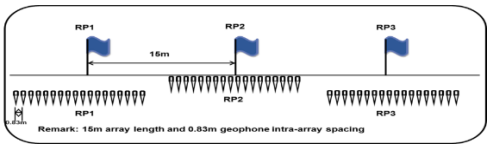

(a)

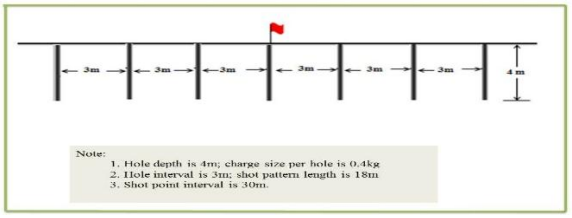

(b)

Figure 5: (a) Receiver Array Configuration and (b) Source Array Configuration

3.2 Ambient Noise and Instrument Test Recording

Daily instrument tests were carried out before the start of each production day to check the performance of the recorder and field digital units (FDU), geophone electronic equipment as well as the ambient noise. The recorder instrumentation noise tests include distortion, gain, phase, common mode, noise, and field impulse. The FDUs noise tests include root-mean-square (rms) noise, phase, distortion, gain, and common mode, and rejection. Geophone were also subjected to such tests as string resistance, leakage, noise and tilt. These tests were routinely carried out three times in a day - start of production in the morning, mid-day and at the end of day's production to ensure acquisition was done within tolerable noise levels. The analyses of the results ensures good geophone coupling, and that the field ground equipment (cables and geophones, FDUs) are performing optimally within the manufacture's specifications and to effect any necessary remediation.

3.3 Data Processing

3.3.1 Noise Detection and Attenuation

Ambient noise detection and attenuation were done using the combination of frequency wavenumber (FK) spectrum analysis and wild amplitude attenuation (WAA) filter tool in GEOEAST Version 2.0 and Vista processing software [21, 27, 28].

3.3.2 Wild Amplitude Attenuation (WAA) Method

Wild amplitude attenuation eliminates the high-amplitude noise which always appears on seismic data such as sonic wave, spike noise, noise burst or erratic noise, power-line noise (50Hz in Nigeria) [29, 30]. WAA filter is based on the idea of "identifying noise on multi-traces and attenuating it from single trace". It automatically recognizes strong noises from seismic data in different bands and determines where these noises occur. The module then suppresses the noise by time variance and spatial variance according to user-defined threshold and attenuation coefficients. The identifying parameter is a transversal weighting median of the seismic data envelope. This method of dividing frequency bands enhanced the high-fidelity of seismic data while attenuating noises.

None of the filters were able to totally remove or attenuate both linear noise and high amplitude noise. Hence the two filters were used in combination. The output of FK filter was used as input for WAA filter. By this process, some of the high amplitude noise that could not be attenuated by FK filtering was attenuated by WAA filtering.

3.3.3 Signal to Noise Ratio (SNR) Computation

Signal to noise calculations were achieved using three different methods. They are Cross Correlation (XC) method, Multi-Coherence (MC) method and Singular Value Decomposition (SVD) method. The method used in this study was the XC method. White and Bekara and Baan have discussed extensively the MC and SVD methods respectively [31,32]. This was achieved by utilizing a time window (milliseconds long) and selected 2 traces wide. Then, it computes correlation datasets referenced to the centre point of the window to estimate the signal to noise. The zero lag value of the auto-correlation of a trace is the sum of the zero lag values of the auto-correlation of a signal and the zero lag value of the auto-correlation of the noise [33]. Signal-to-noise (SNR) was calculated from the seismic sections of Lines AA", BB" and CC" (Figure 5) at each Common Depth Point (CDP) using a time window of 1000 to 2000ms. The SNR computation was done on both seismic sections with de-noise filter applied and the seismic section without the application of de-noise filter.

4. RESULTS AND DISCUSSION

4.1 Background Noise

4.1.1 Background Noise Identification on Shot Gathers

Observed noise sources during seismic data acquisition are presented in Figures 6 - 11.

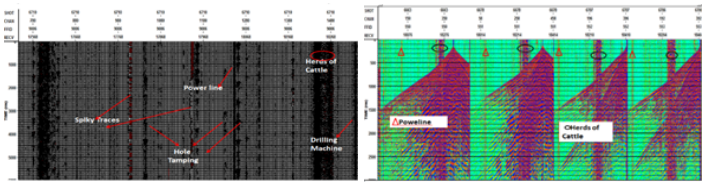

(a) (b)

Figure 6: (a) Example of background noise data showing spiky traces, power line, hole tamping, herds of cattle and drilling machine noise and (b) Raw shot gather showing power line cattle noise.

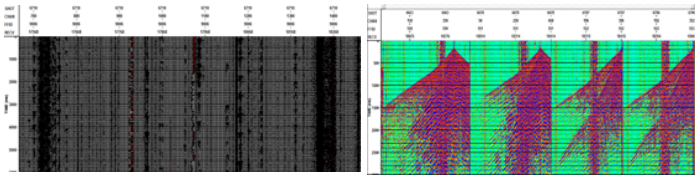

(a) (b)

Figure 7: (a) Sample Acquired Data without Signal Generation (Background Noise) and (b) Sample Acquired Data with Signal Generation (Raw Shot Gather Display).

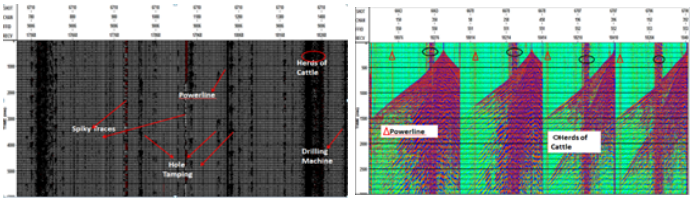

(a) (b)

Figure 8: (a) Data with Sources of Noise on Background Noise Display and (b) Data with Powerline and Herds of Cattle Noise on Raw Shot Gather.

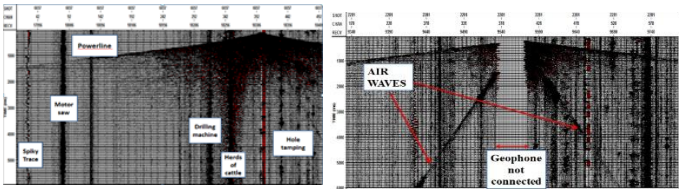

Figure 9: (a) Data with spiky trace, motor-saw noise, powerline, drilling machine and hole tamping noises on a Raw Shot Gather and (b) Data with airwaves and bad geophones on a Raw Shot Gather.

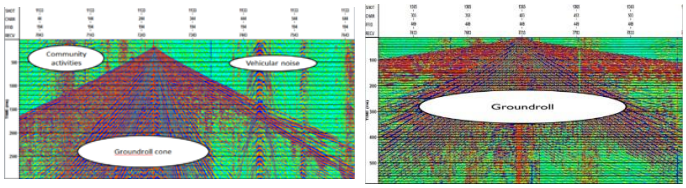

Figure 10: (a) Data with community activities, groundroll and vehicular noise on a Raw Shot Gather and (b) Data with Groundroll noise on Raw Shot Gather.

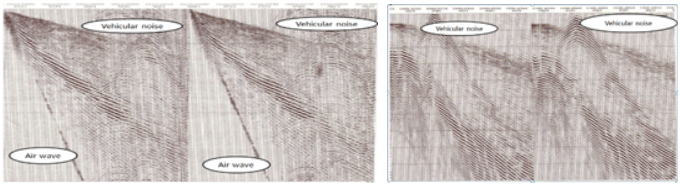

(a) (b)

Figure 11: (a) Data with air waves and vehicular noise on a Raw Shot Gather and (b) Data with Vehicular noise on a Raw Shot Gather.

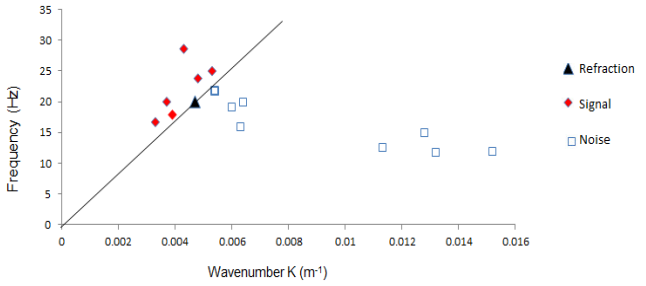

Figure 12: Plot of Frequency against Wavenumber from Table 2.

Figures 13 - 15 are plots of noise level from the field sensor tests against geophone stations and histogram plots of spread noise level distribution for lines AA", BB" and CC". Figures 16 – 18 are plots of resistance, tilt and leakage against geophone stations for Lines AA", BB" and CC" (Figure 4).

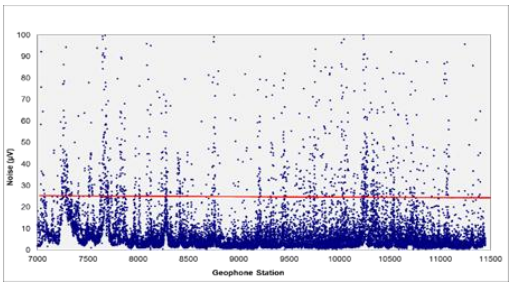

(a)

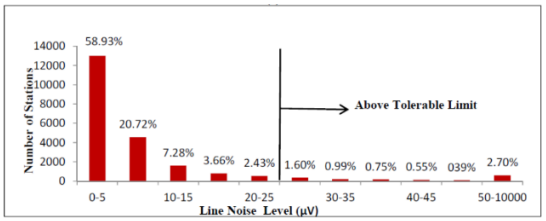

(b)

Figure 13: (a) Plots of Noise Level against Geophone stations for Line AA" and (b) Histogram Plots of Line AA" Spread Noise Level Distribution.

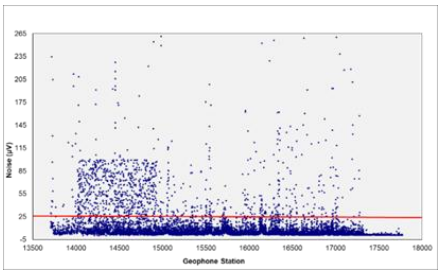

(a)

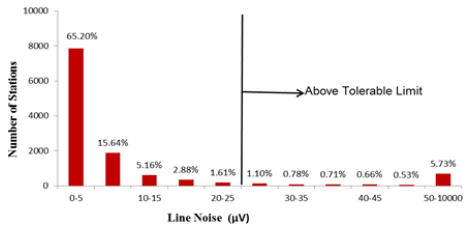

(b)

Figure 14: (a) Plot of Noise Level Against Geophone stations for Line BB" and (b) Histogram Plots of Line BB" Spread Noise Level Distribution.

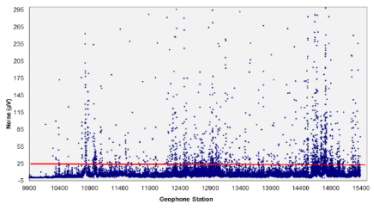

(a)

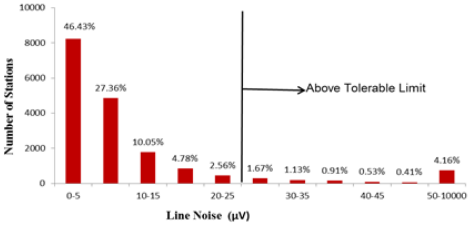

(b)

Figure 15: (a) Plots of Noise Level against Geophone stations for Line CC" and (b) Histogram Plots of Line CC" Spread Noise Level Distribution.

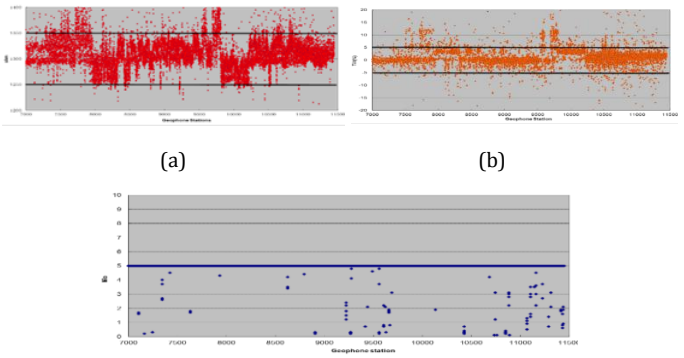

(a) (b)

(c)

Figure 16: Showing Plots of (a) Resistance, (b) Tilt and (c) Leakage against Geophone stations for Line AA"

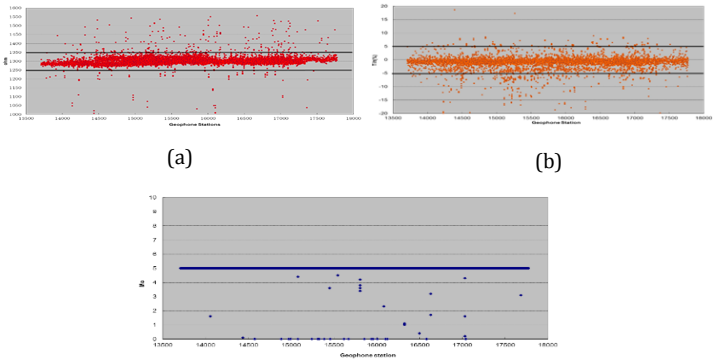

(a) (b)

(c)

Figure 17: Showing Plots of (a) Resistance, (b) Tilt and (c) Leakage against Geophone stations for Line BB"

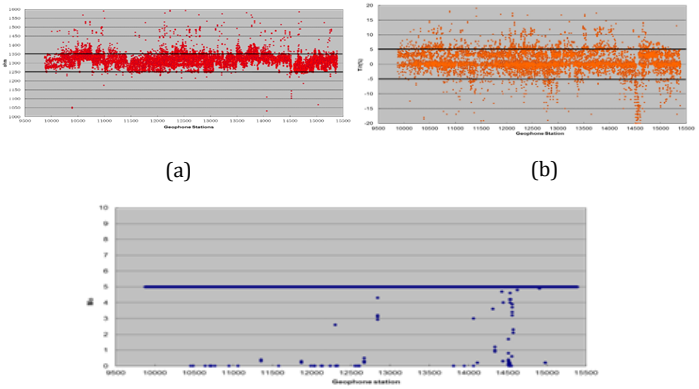

(a) (b)

(c)

Figure 18: Showing Plots of (a) Resistance, (b) Tilt and (c) Leakage against Geophone stations for Line CC"

4.2 Spectral Analyses

The results of spectral analyses of various type of noise within the study area are presented in Figures 19 - 28.

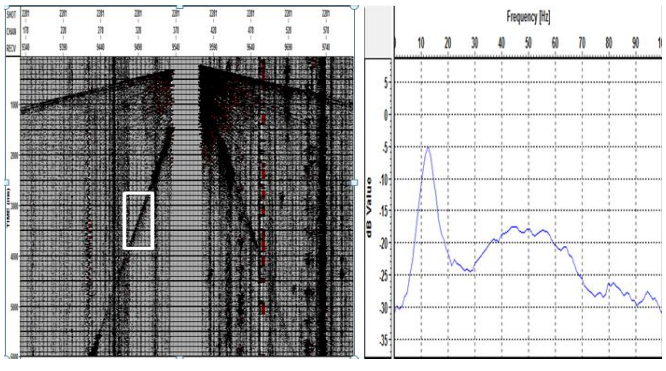

(a) (b)

Figure 19: (a) Raw Shot Gather Display showing the area selected for Airwave Noise analysis in white box and (b) the Amplitude Spectrum of Airwave Noise in dB.

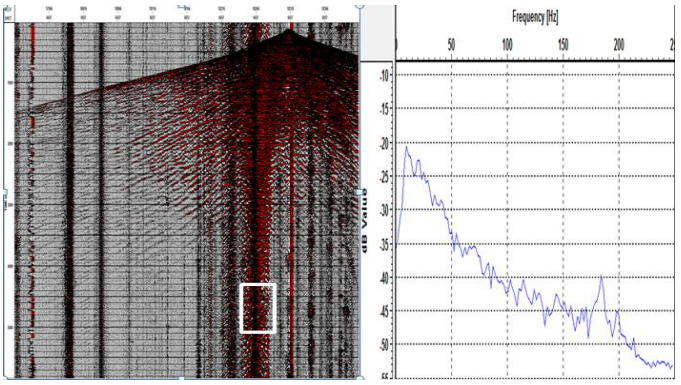

(a) (b)

Figure 20: (a) Raw Shot Gather Display showing the area selected for Herds of Cattle Noise analysis in white box and (b) the Amplitude Spectrum of Herds of Cattle Noise in dB.

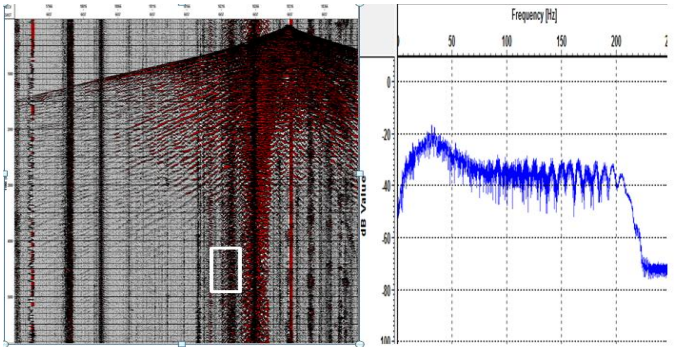

(a) (b)

Figure 21: (a) Raw Shot Gather Display showing the area selected for Drilling Machine Noise analysis in white box and (b) the Amplitude Spectrum of Drilling Machine Noise in dB.

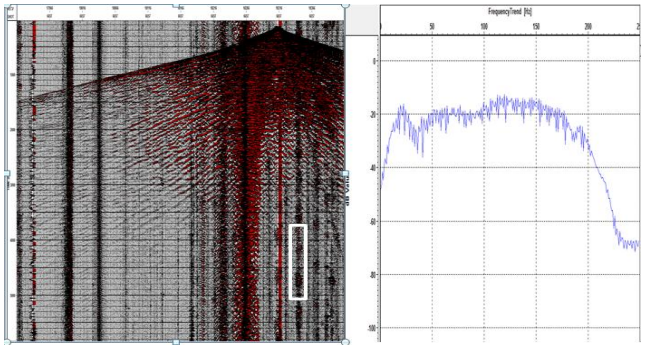

(a) (b)

Figure 22: (a) Raw Shot Gather Display showing the area selected for Hole-Tamping Noise analysis in white box and (b) the Amplitude Spectrum of Hole-Tamping Noise in dB.

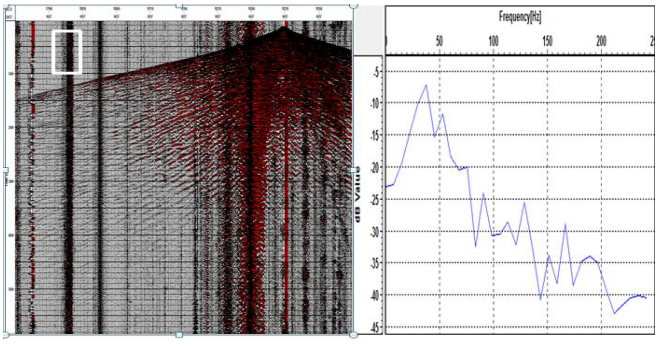

(a) (b)

Figure 23: (a) Raw Shot Gather Display showing the area selected for Motor-saw Noise analysis in white box and (b) the Amplitude Spectrum of Motor-saw Noise in dB.

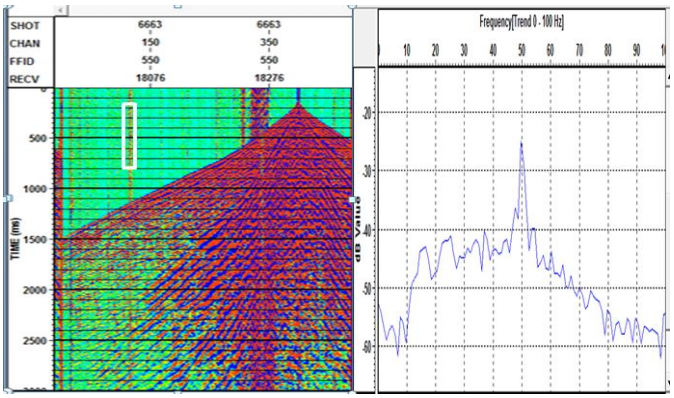

(a) (b)

Figure 24: (a) Raw Shot Gather Display showing the area selected for Power-line Noise analysis in white box and (b) the Amplitude Spectrum of Power-line Noise in dB.

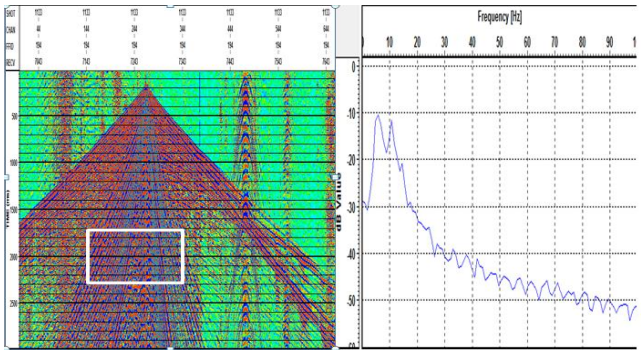

(a) (b)

Figure 25: (a) Raw Shot Gather Display showing the area selected for Ground roll Noise analysis in white box and (b) the Amplitude Spectrum of Ground roll Noise in dB.

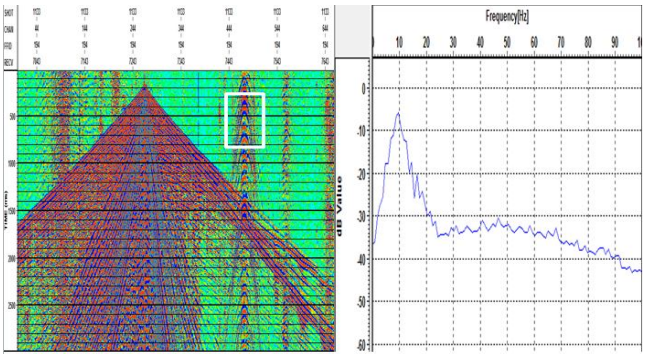

(a) (b)

Figure 26: (a) Raw Shot Gather Display showing the area selected for Vehicular Noise analysis in white box and (b) the Amplitude Spectrum of Vehicular Noise in dB.

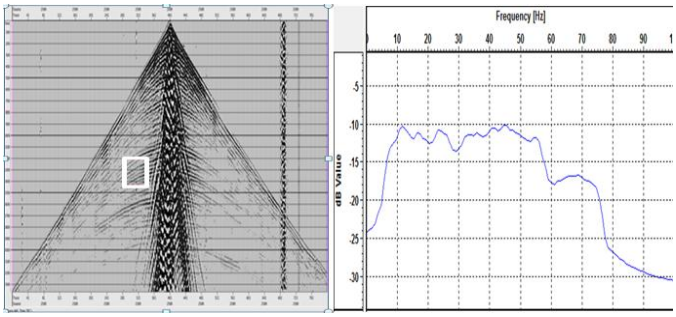

(a) (b)

Figure 27: (a) Raw Shot Gather Display showing the area selected for Signal analysis in white box and (b) the Amplitude Spectrum of Signal in dB.

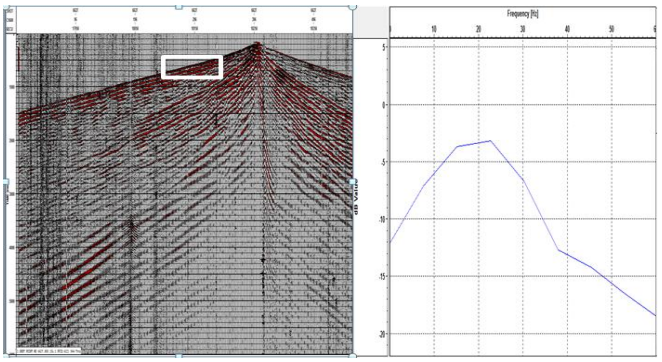

(a) (b)

Figure 28: (a) Raw Shot Gather Display showing the area selected for Refraction (First break) analysis in white box and (b) the Amplitude Spectrum of Refraction (First break) in dB

4.3.1 Signal and Noise Dominant Frequencies and Amplitudes

The dominant frequencies /amplitudes of various noise sources and signals are presented in Table 1.

Table 1: Results of Various Noise Sources with Dominant Frequencies/Amplitudes from Plots of Amplitude Spectral Analyses.

Source	Frequency (Hz)	Amplitude (dB)
Motor-saw	15 - 70	(-22 to -7)
Airwave	8 - 19	(-25 to -5)
Ground-roll	6 - 17	(-30 to -11)
Herds of cattle	5 - 50	(-33 to -21)
Vehicles	6 - 20	(-35 to -6)
Hole-tamping	25 - 70	(-25 to -18)
Powerline	50	(-42 to -25)
Drilling Machine	20 - 60	(-30 to -20)
Signal	6 - 75	(-20 to -10)
Refraction	4 - 35	(-10 to -3)

4.4 Noise Attenuation Schemes

4.4.1 Noise Removal from Raw Shot Gathers

Presented in Figure 29 is a representative of the noise removals from six raw shot gathers using frequency wavenumber number (FK) and wild amplitude attenuation (WAA) filters [30]. Figures 30 is a representative display of removing both linear and ambient noise from fourteen raw shot gathers using the combination of frequency wave number and wild amplitude filters.

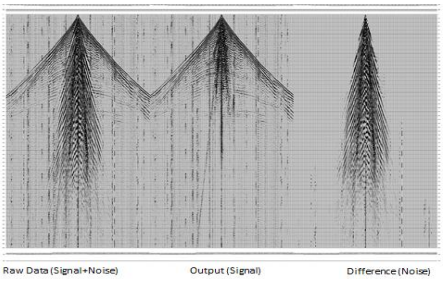

(a)

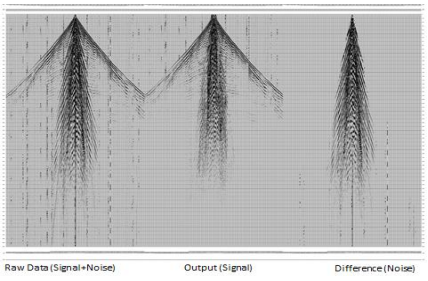

(b)

Figure 29: Representative of Noise Removal Schemes using (a) FK Filter and (b) WAA filter at a Shot point separately.

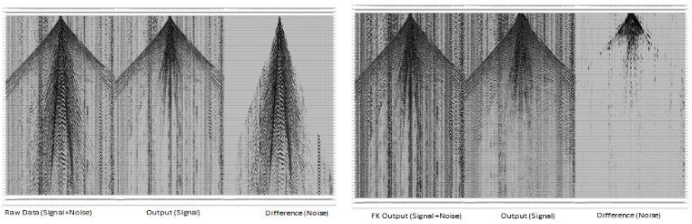

(a) (b)

Figure 30: Representative of Noise Removal Schemes using combination of (a) FK Filter and (b) WAA filter at a Shot point

4.4.2 Noise Removal from Stack Sections

Presented in Figures 31 – 33 are the result of the application of noise removal filters to stack section of Lines AA", BB" and CC".

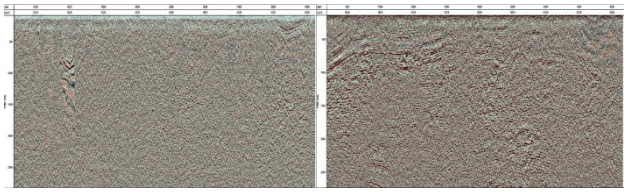

(a) (b)

Figure 31: Brute Stack Section (a) Before Noise Attenuation (Without Filter Applied) and (b) After Noise Attenuation (With Filter Applied) for Line AA"

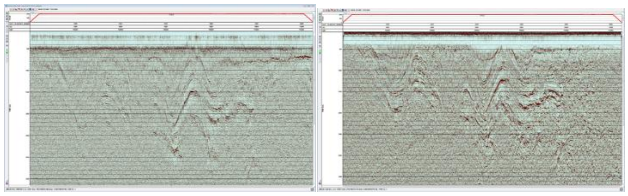

(a) (b)

Figure 32: Brute Stack Section (a) Before Noise Attenuation (Without Filter Applied) and (b) After Noise Attenuation (With Filter Applied) for Line BB"

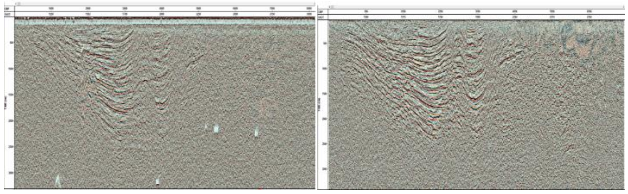

(a) (b)

Figure 33: Brute Stack Section (a) Before Noise Attenuation (Without Filter Applied) and (b) After Noise Attenuation (With Filter Applied) for Line CC"

4.3.3 Background Noise

Notably sources of noise prevalent in the research area were vehicular noise, powerline, community activities, Lumbering/timbering activities, herds of cattle, ground roll, airwaves, direct arrivals, hole tamping, noise emanating from drilling machines and refraction. Most of these noises appeared pre first break and continues to the end of data record as shown in Figures 6 – 11, thereby suggesting that they are not source-generated (the noise would be present whether we were shooting or not). It contaminates the data quality.

Figures 7 (a and b) are samples of raw shot gather displays showing acquired data without signal generation and data with signal generation. Figure 7a was acquired when field sensor tests was conducted to know the level of ambient (background) noise within the active spread in the study area before commencement of normal production. Figure 7b was acquired during a normal production. The vertical axis is the two-way travel time and the horizontal axis is the shot offset distance. The top label gives the corresponding values of the shot points, channel numbers, receiver stations and field file numbers for easy identification.

Figures 8 - 11 are raw shot gather displays showing various types of noise. The noise emanating from hole-tamping (covering of charge size with earth after loading) occurs every 500ms with high amplitude from a two-way travel time display shown in Figures 8a and 9a. This particular noise that contaminates the data can be controlled by stopping the loading crew when a shot is to be taken.

4.3.4 Source-Generated Noise

Figures 9 – 11a show the air wave, refraction, direct arrivals and ground roll noise recorded in the study area. These noises do not appear pre first-break but started immediately after first-break and continues till end of data record, thereby suggesting that they are source generated (the noise would not be present if we weren't shooting). It contaminates the data quality. They are coherent noise and are predictable from trace to trace across a group of traces because they have a phase relationship between adjacent traces. The air wave in Figure 9 is mostly caused by a blow-out of the shot which is not properly tamped. It is obvious that reflection is covered with a blanket of ground-roll as shown in Figure 10. Analysis of the ground roll noise shows that it has two distinct modes with velocities around 400ms^{-1} and 810 ms^{-1} both of which are dispersive with wavelength (λ) of 61.5m. The ground-roll wave train can be most disruptive energy and therefore calls for some kind of action to remove it so as to improve the SNR.

4.3.5 Signal and Noise Characterization/Identification

Signal and noise were recognized according to its calculated characters as shown in Table 2. Reflected signals are characterized by their velocity, which is always greater than that of the noise. We considered the fact that the first refraction is propagating with the velocity of the first subsurface layer, and not with that of the surface layer and its value is 4232 ms^{-1}. The velocity of the first refraction is evidently greater than that of the surface layer, hence greater than that of the noise. This is because velocity generally increases with depth and subsurface layer is deeper than surface layer.

Table 2: Signal and Noise Identification

Serial Number	Distance, dx (m)	Time, dt (ms)	Period, T (ms)	Velocity V (ms^{-1})	Wavelength, λ (m)	Wavenumber K (m-1)	Frequency F (Hz)	Identification
1	550	130	50	4231	211.6	0.0047	20	Refraction
2	250	280	85	893	75.9	0.0132	11.8	Noise
3	350	300	67	1167	78.2	0.0128	14.9	Noise
4	200	37	50	5405	270.3	0.0037	20	Signal
5	300	120	63	2500	157.5	0.0063	15.9	Noise
6	250	54	56	4630	259.3	0.0039	17.9	Signal
7	400	84	40	4762	190.5	0.0053	25	Signal
8	400	78	60	5128	307.7	0.0033	16.7	Signal

9	300	379	83	792	66	0.0152	12	Noise
10	750	678	80	1106	88.5	0.0113	12.5	Noise
11	200	50	46	4000	184	0.0054	21.7	Noise
12	400	60	35	6667	233.3	0.0043	28.6	Signal
13	250	80	50	3125	156.3	0.0064	20	Noise
14	600	187	52	3209	166.8	0.006	19.2	Noise
15	200	40	42	5000	210	0.0048	23.8	Signal
Mean	360	170.467	57.267	3507.667	177.060	0.007	18.667	
Stdev	162.788	175.994	15.641	1865.887	75.260	0.004	4.898	

Figure 12 is a graph of frequency versus wavenumber from the analysis of signal and noise identification. This graph represents the different remarked events from the noise analysis shown in Table 2. The identified first arriving refraction event is represented here in black colour as shown in Figure 12. The line passing by it to the origin point makes a separation between the useful reflected energy (red marks) and the unwanted noise (empty squares). Signals are closer to the F-axis, while noise is closer to the K-axis. The graph enables to distinguish between the noise and signal. Events with velocities greater than the first refraction's velocity are considered as signals. The events with less velocity are noise.

4.3.6 Noise Attenuation

Figure 29a shows displays of noise removals from three raw shot gathers using frequency wavenumber number (FK) filtering algorithm. There are three displays for each raw shot gather. The first display on the left is the raw shot gather (contains the signal and noise). The second display in the middle is the output (signal) while the third display on the right is the difference obtained by subtracting output from the input (noise).

The FK filter was designed to cut off linear events with frequencies below 17Hz and wavenumber (K) ranging from -0.1 to +0.1 from the frequency wavenumber spectrum. The cut off or mute frequency used in the FK filter design was based on the known low frequency characteristics of ground roll noise (usually <17Hz) as displayed in Figure 25. Some useful low frequency signals might have been destroyed by the application of this filter because there is usually a frequency overlap between ground-roll and the signals. Their destruction is very minimal since they were still very visible after the filtering. However, there still appears random noise on the data after filtering. The best efficient method to attenuate random noise from seismic dataset is through stacking. To improve noise separation from the raw shot gather, we applied wild amplitude attenuation (WAA) filter.

WAA algorithm was also applied to the same raw shot gathers for comparison, given the results shown in Figure 29b. Comparing the results (filtered output) obtained with the WAA and FK filtering, it is obvious that WAA filters could not effectively remove linear noise from seismic data unlike the FK filters. But WAA filter is better at attenuating high amplitude noise (i.e. spike noise, erratic noise, etc.) than is the FK filter.

However, some high amplitude noise that could not be attenuated by FK filters was removed by WAA filtering. Hence, the combination of these two filters (FK and WAA) was employed in attenuating both linear and high amplitude noises as displayed in Figure 8. The output data from FK filter was used as input data for WAA filter and the result obtained after the combination of the two filtering algorithms showed the signals more clearly and better enhanced. The resulting enhancement of the SNR clearly improves interpretation of the raw shot gather as shown in Figure 8.

4.3.7 Standard Signal Spectrum

Figure 27 shows the signal spectrum obtained in the study area. The dominant amplitude of the primary reflections (signals) ranges between -20dB to -10dB, while its dominant frequency varies from 6Hz to 75Hz. The amplitude of the primary reflections and seismic noise are significantly different as shown in Table 4.6 and Figures 19 - 28.

4.3.8 Signal-to-Noise Ratio (SNR)

The values of amplitudes obtained during the estimation of signal-to-noise ratio across 269 selected traces with different mid-point at time windows of 1000ms, 1500ms and 2000ms were computed from both filtered and unfiltered brute stack sections of Lines AA", BB" and CC". The filtered amplitude values are much higher than the values of the unfiltered amplitudes, indicating that SNR are highest when noises are attenuated from the data than when noise algorithm is not applied to the data. The mean values of the filtered and unfiltered amplitudes are 1.61 and 0.80 respectively with an average difference of 0.81. Thus, the SNR was improved at an average of 0.81 after noise attenuation. The highest amplitude value was 3.38.

Figures 31a, 32a and 33a are stack sections without applying any noise removal algorithm except incoherent noise that cancels out during stacking process. After applying the combination of the FK and WAA filters to the same sections, the resulting sections were greatly improved as structural features are more clearly seen. This is shown in Figures 31b, 32b and 33b. Thus, the SNR were greatly improved. This is evident from the graph of amplitude against CMP number shown in Figure 34. Generally, the amplitudes of both the filtered and unfiltered seismic sections increase slightly as we sample across CMP traces.

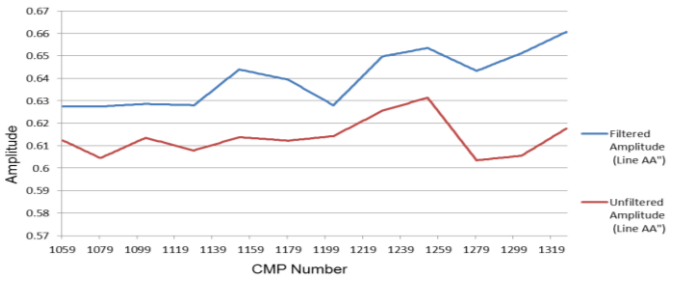

(a)

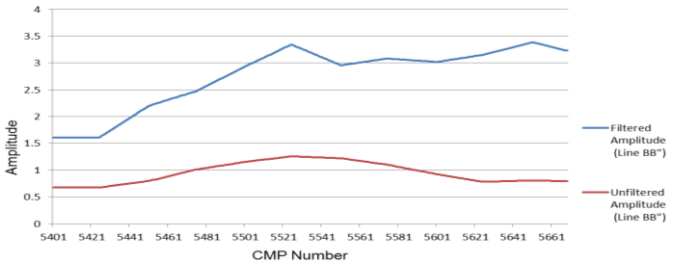

(b)

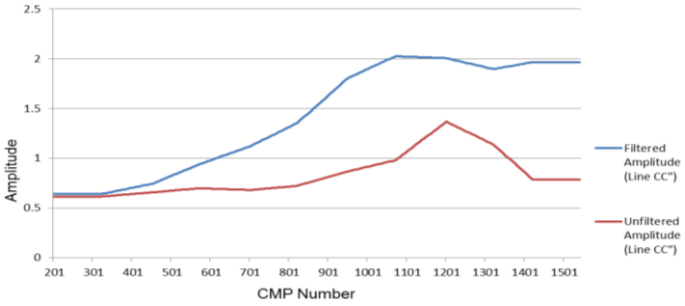

(c)

Figure 34: Plots of Amplitude Against Common Mid-Point (CMP) Number (a) Line CC", (b) Line BB" and (c) Line AA". (Graphs of SNR at 100ms, 1500ms and 2000ms for lines AA", BB" and CC" respectively)

4.3.9 Field Sensor Tests

The noise values varied from 0.3μV to 6238μV. The averages of the three 2D traverse line noises are 13.37μV for line AA", 13.52μV for line BB" and 15.59μV for line CC", and the mean noise for the three traverse line is 14.16μV. The standard deviations of the means are 95.44μV, 87.62μV and 67.17μV for lines AA", BB" and CC" respectively. The highest noise level values of 5477μV, 6238μV and 2311 μV are recorded at geophone stations 10207, 15707 and 14015 from traverse lines AA", BB" and CC" respectively. These geophone stations are located in the Fulani camp settlements and the values indicate burst noise or erratic noise emanating from bad channels. The geophone coil resistance values range from 3.37Ω to 2558.8Ω. The averages of the three 2D traverse line geophone coil resistance are 1319.71Ω for line AA", 1296.16Ω for line BB" and 1299.28Ω for line CC", and the mean resistance for the three traverse line is 1305.05Ω.

The geophone leakage and tilt values range from (0 – 5) Mo and -99.8% to 100% respectively. The means are 4.98Mo and 0.68% while the standard deviations are 0.30Mo and 7.62%. Figures 13 - 15 are plotted from the values of receiver point numbers. These are the background noise prevalent in the study area without explosive detonation and do not include the ambient seismic noise generated as a result of explosive detonation. The graph shows a cluster of ambient noise level between 0 to 5 μV across the active spread in Lines AA", BB" and CC". Figures 13 – 15 show the noise values that are within and those that are above tolerable noise limit of <25μV. It is a standard practice that the tolerance noise limit acceptable in seismic data acquisition is that 15 % of the active traces should not exceed 25μV [9]. It is evident from Figures 13 – 15 that 93.02%, 90.49% and 91.18% of traces in Lines AA", BB" and CC" respectively with average of 91.56% are below 25μV which is the tolerance noise level limit. The total number of traces obtained in this passive noise analysis that exceeded the acceptable noise limit was 8.44%. This indicates that the ambient seismic noise level excluding source generated noise is within the acceptable limit prior to start of each days recording production. Figures 16 – 19 show the values of resistance, tilt and leakage that are within defined specification and those that are out of specification.

4.3.10 Various Noise Spectra

Figures 16 – 28 illustrate the amplitude and frequency relationship of the ambient seismic noise while the summary of various noise sources with dominant frequencies / amplitudes are shown in Table 1. The dominant amplitude of the vehicular noise varies from -35dB to -6dB, while its dominant frequency varies between 6Hz and 20Hz. The powerline noise frequency is 50Hz with corresponding peak amplitude of -25dB. Airwave has its dominant amplitude and frequency varying between -25dB to -5dB and 8Hz to 19Hz respectively. Its velocity is 330m/s with apparent wavelength of 27.5m. Airwave peak frequency from Figure 16 is 12Hz.

The dominant amplitude of ground rolls ranges between -30db and -11dB, while its dominant frequency varies from 5Hz to 17Hz with peak frequency at 6.5Hz as shown in Figure 25. These ground roll parameters are useful in the source and receiver array design for seismic data acquisition. The dominant frequency and amplitude of the herds of cattle ranges from 5Hz to 50Hz and -33dB to -21dB respectively. The dominant amplitude ranges of refraction, drilling machine, hole-tamping and motor-saw ranges from -10dB to -3dB, -30dB to -20dB, -25dB to -18dB and -22dB to -7dB respectively.

It is evident from Figures 16 - 28 that the dominant amplitude of ambient seismic noise ranges from -42dB to -3dB, while its dominant frequency varies from 4Hz to 70Hz. Ambient seismic noise can be attenuated from the seismic section by utilizing its frequency and amplitude characteristics as stated above. By inputting these parameters in the attenuation algorithm during seismic data processing, it would image subsurface geology better, thus the risk of drilling dry oil wells will be reduced.

Source depth affects seismic noise pattern and in order to reduce seismic noise, especially source generated noise (ground roll), sources are placed below the weathered zone [20, 11]. The data acquired in the area were masked with surface wave noise especially ground rolls and airwaves (see Figures 10). This was due to the fact that the source depth (4.0m) were placed in unconsolidated layer and most of the energy while escaping to the surface generated ground rolls and airwaves resulting from blowouts. Hence the transmitted seismic energy was not maximized. To effectively reduce the noise emanating from ground roll in the field during seismic data acquisition, we should bury the source (explosives) below the weathering layer or adopt smaller charges.

5. CONCLUSION

Having a successful field technique requires the knowledge of the characteristics of the ambient seismic noise in relation to the desired signal, and its removal from the seismogram necessitates the determination of its character and strength. The following conclusions are drawn from this work. The dominant amplitude of the primary reflection ranges between -20dB to -10dB, while those of the ambient seismic noise, varies between -42dB to -3dB. Also, the primary reflections had its dominant frequency varying from 6Hz to 75Hz while that of ambient seismic noise varies between 4Hz to 70Hz.

Analysis of the noise shows two distinct ground roll modes with velocities around 400 m/s and 810 m/s both of which are dispersive with wavelength (λ) of 61.5m and peak frequency at 6.5Hz. The characteristics of seismic noise established in this study is relevant because when ambient seismic noise is to be attenuated or removed from a seismic section, it would be required as inputs in the attenuation algorithm, which would result in an improved imaging of the subsurface, thereby reducing the risk of drilling dry oil wells.

By combining FK and WAA filters, surface waves especially ground rolls and other high amplitude noises were effectively attenuated making the primary reflection very visible and better enhanced. The resulting enhancement of the SNR clearly improves interpretation of the seismic data. The filtered amplitude values are much higher than the values of the unfiltered amplitudes indicating that SNR are highest when noises are attenuated from the data than when noise algorithm is not applied to the data. Consequently, the data acquired were masked with surface wave noise especially ground rolls and airwaves. Having placed the source depth in an unconsolidated layer, most of the energy while escaping to the surface, caused blowouts generating ground rolls and airwaves. Hence the transmitted seismic energy was not maximized. The introduction of the wide amplitude attenuation (WAA) filter showed that the signals are more clearly and better enhanced. This was the first time of using the filter in the area.

ACKNOWLEDGEMENTS

The authors are grateful to Frontier Exploration Services (FES), a subsidiary of Nigeria National Petroleum Corporation (NNPC) for the data.

REFERENCES

[1] Anderson, R., McMechan, G. 1989. Automatic editing of noisy seismic data. Geophysical Prospecting, 37, 875-892.

[2] Stewart, R.R. 1998. Air-noise reduction on geophone data using microphone records: Consortium for Research in Elastic Wave Exploration Seismology (CREWES) Research Report, 10, 67-77.

[3] Boonefoy-Claudet, S., Cotton, F., Pierre-Yves, B. 2006. The nature of noise wavefield and its application for site effects studies, Earth - Science Reviews, 1-23.

[4] Chen, K. 2013. Robust matrix rank reduction methods for seismic data processing. Unpublished M. Sc. Dissertation, University of Alberta.

[5] Trickett, S., Burroughs, L., Milton, A. 2012. Robust rank reduction filtering for erratic noise, 82nd Annual International Meeting, SEG, Expanded Abstracts, 1-5.

[6] Afegbua, K.U., Ezomo, F.O. 2013. A preliminary investigation of the signal-to-noise ratio of Toro and Nsukka stations in Nigeria. International Journal of Physical Sciences, 8 (16), 707-716.

[7] Normark, E. 2011. Wind and rain induced noise on reflection seismic data, Near Surface 2011 - 17th EAGE European Meeting of Environmental and Engineering Geophysics.

[8] Dean, T. 2019. The seismic signature of rain. American Society of Exploration Geophysicist Extended (ASEG) Abstracts.

[9] Lengeling, R. 2003a. Ambient noise analysis part 1. Schlumberger WesternGeco.

[10] Lengeling, R. 2003b. Ambient noise analysis part 2. Schlumberger WesternGeco.

[11] Uko, E.D., Ekine, A.S., Ebeniro, J.O., Ofoegbu, C.O. 1992. Weathering structure of the east-central Niger Delta, Nigeria. Geophysics, 57 (9), 1228-1233.

[12] Eze, C.L., Okwueze, E.E., Uko, E.D. 2003. The velocity-thickness characteristics of the mangrove swamp low velocity layer (LVL) South central Niger Delta, Nigeria. Global Journal of Pure and Applied Sciences, 9 (3), 369-374.

[13] Ukaonu, C., Ukaigwe, F. 2004. Dispersion pattern of ground roll (seismic noise) in Eastern Niger Delta. Society of Petroleum Engineers, 2, 1-14.

[14] Aigbedion, I. 2007. Dispersion patterns of ground roll (seismic noise) in Northern Niger delta Nigeria. Journal of Applied Sciences, 7 (2), 175-181.

[15] Dagogo, T., Ebeniro, J.O. 2015. Shallow subsurface characterization using multi-channel analysis of surface waves in the Niger Delta. International Journal of Emerging Knowledge, 3 (2), 31 – 38.

[16] Ugwu, S.A., Nwankwo, C.N., Sule, J.O. 2017. Characterization of ground rolls in the North-West of Niger Delta Nigeria, West Africa, Egyptian. Journal of Petroleum, 27, 541-552.

[17] Mbachi, C.N.C., Uko, E.D., Ngeri, A.P., Ofoegbu, C.O. 2018. Estimation of the Dipping Angles of Refractors in the Middle Benue Trough Nigeria Using Generalized Reciprocal Method. Asian Journal of Applied Science and Technology, 2 (4), 10-22.

[18] Mgbemere, P.C., Uko, E.D., Mbachi, C.N.C., Tamunobereton-ari, I., Ofoegbu, C.O., Ngeri, A.P. 2018. Mapping of depth to bedrock in the Middle Lower Benue Trough Nigeria, using Seismic Refraction Method. Journal of Applied Geology and Geophysics, 6 (5), 05-14.

[19] Umoetok, D.B., Uko, E.D., Ngeri, A.P. 2019. Attenuation of Water-Bottom Multiples: A Case Study from Shallow Marine in the Niger Delta, Nigeria. Malaysian Journal of Geosciences, 3 (1), 61-65.

[20] Jolly, R.N., Mifsud, J.F. 1971. Experimental Studies of Source-Generated Seismic Noise. Geophysics, 36 (6), 1138-1149.

[21] Yilmaz, O. 1991. Velocity-stack processing: Geophysical Prospecting, 37, 357–382.

[22] Avbovbo, A.A. 1980. Basement Geology in the Sedimentary Basins of Nigeria. Geology, 8, 323-327.

[23] Obaje, N.G. 1996. Potential for coal-derived gaseous hydrocarbons in the middle Benue Trough of Nigeria. Journal of Petroleum Geology, 19, 77-94.

[24] Obaje, N.G. 2009. Geology and Mineral Resources of Nigeria. Lecture Notes in Earth Sciences. Springer-verlag, Berlin, Heildeberg, 120, 57-68.

[25] Whiteman, A.J. 1982. Nigeria its Petroleum Geology, Resources and Potential 1, Graham and Trotman: London, UK.

[26] Fatoye, F.B., Gideon, Y.B. 2013. Geology and mineral resources of Benue trough, Nigeria. Advances in Applied Science Research, 4(6), 2-28.

[27] Zhou, B., Greenhalgh, S.A. 1994. Wave-equation extrapolation-based multiple attenuation: 2-D filtering in the f-k domain. Geophysics, 59, 1377–1391.

[28] Adizua, O.F., Inchinbia, S., Ekine, A.S. 2017. Design of an Optimal High Pass Filter in Frequency - Wave Number (F-K) Space for Suppressing Dispersive Ground Roll Noise from Onshore Seismic Data. Universal Journal of Physics and Application, 11 (5), 144–149.

[29] Schlumberger Training Manual. 2009. Schlumberger WesternGeco Training Manual on Data Processing Dubai.

[30] Wang, Z., Xue, X., Li, X., Jiang, Z., Reddy, K. 2018. Study on Attenuation Properties of Surface Wave of AE Simulation Source Based on OPCM Sensor Element. Journal of Sensors, ID 6926594, 1-6.

[31] White, R.E. 1973. The Estimation of Signal Spectra and Related Quantities by Means of the Multiple Coherence Function, Geophysical Prospecting, 21, 660-703.

[32] Bekara, M., Baan, V.D. 2007. Local singular value decomposition for signal enhancement of seismic data. Geophysics, 72 (2), V59-V65.

[33] Harker, B.M., Gee, K.L., Neilsen, T.B., WallMcInerny, A.T., McInerny, S.A., James, M.A. 2013. On autocorrelation analysis of jet noise. Journal of Acoustic Society of America, 133, EL458, doi: 10.1121/1.4802913.